Title
Mice lacking sialyltransferase ST3Gal-II develop late-onset obesity and insulin resistance.

Journal
Glycobiology, 27(2)

ISSN
0959-6658

Authors
Lopez, Pablo Hh
Aja, Susan
Aoki, Kazuhiro
et al.

Publication Date
2017

DOI
10.1093/glycob/cww098

Peer reviewed

Glycobiology, 2017, vol. 27, no. 2, 129–139
doi: 10.1093/glycob/cww098
Advance Access Publication Date: 16 December 2016
Original Article

OXFORD

Cell Biology

Mice lacking sialyltransferase ST3Gal-II develop late-onset obesity and insulin resistance

Pablo HH Lopez[2,8], Susan Aja[3,4], Kazuhiro Aoki[5], Marcus M Seldin[3,6], Xia Lei[3,6], Gabriele V Ronnett[3,4,6,7], G William Wong[3,6], and Ronald L Schnaar[1,2,4]

[2]Department of Pharmacology and Molecular Sciences, [3]Center for Metabolic and Obesity Research, [4]Department of Neuroscience, Johns Hopkins University School of Medicine, Baltimore, MD 21205, USA, [5]Complex Carbohydrate Research Center, University of Georgia, Athens, GA 30602, USA, [6]Department of Physiology, and [7]Department of Biological Chemistry, Johns Hopkins University School of Medicine, Baltimore, MD 21205, USA

[1]To whom correspondence should be addressed: Tel: 1-410-955-8392; e-mail: schnaar@jhu.edu

[8]Present address: Instituto de Investigación Médica Mercedes y Martin Ferreyra-INIMEC-CONICET-Universidad Nacional de Córdoba, Friuli 2434, Barrio Colinas de Velez Sarsfield, Ciudad de Córdoba, Córdoba CP 5016, Argentina.

Received 15 July 2016; Revised 22 September 2016; Accepted 26 September 2016

Abstract

Sialyltransferases are a family of 20 gene products in mice and humans that transfer sialic acid from its activated precursor, CMP-sialic acid, to the terminus of glycoprotein and glycolipid acceptors. ST3Gal-II (coded by the *St3gal2* gene) transfers sialic acid preferentially to the three positions of galactose on the Galβ1-3GalNAc terminus of gangliosides GM1 and GD1b to synthesize GD1a and GT1b, respectively. Mice with a targeted disruption of *St3gal2* unexpectedly displayed late-onset obesity and insulin resistance. At 3 months of age, *St3gal2*-null mice were the same weight as their wild type (WT) counterparts, but by 13 months on standard chow they were visibly obese, 22% heavier and with 37% greater fat/lean ratio than WT mice. *St3gal2*-null mice became hyperglycemic and displayed impaired glucose tolerance by 9 months of age. They had sharply reduced insulin responsiveness despite equivalent pancreatic islet morphology. Analyses of insulin receptor (IR) tyrosine kinase substrate IRS-1 and downstream target Akt revealed decreased insulin-induced phosphorylation in adipose tissue but not liver or skeletal muscle of *St3gal2*-null mice. Thin-layer chromatography and mass spectrometry revealed altered ganglioside profiles in the adipose tissue of *St3gal2*-null mice compared to WT littermates. Metabolically, *St3gal2*-null mice display a reduced respiratory exchange ratio compared to WT mice, indicating a preference for lipid oxidation as an energy source. Despite their altered metabolism, *St3gal2*-null mice were hyperactive. We conclude that altered ganglioside expression in adipose tissue results in diminished IR sensitivity and late-onset obesity.

Key words: adipose tissue, ganglioside, hyperglycemia, metabolism, sialic acid

Introduction

Sialic acids are abundant terminal saccharides on glycoproteins and glycolipids that dominate the cell surfaces of vertebrate cells and tissues (Cohen and Varki 2010). Sialoglycans are synthesized by the action of sialyltransferases, a family of 20 enzymes (in mice and humans) that transfer sialic acid from the activated donor CMP-sialic acid, to the glycan terminus of a glycolipid or glycoprotein (Audry et al. 2011). The functions of sialoglycans are diverse (Schauer 2009; Bauer and Osborn 2015);

phenotypes associated with genetic disruptions in sialyltransferase genes in mice and humans are beginning to reveal the functions of their sialoglycan products (Taniguchi et al. 2014).

Among sialoglycans, gangliosides—sialylated glycosphingolipids—are found at varying densities and structural complexity in all mammalian tissues (Iwamori et al. 1984), where they regulate cell function and mediate intracellular recognition (Todeschini and Hakomori 2008). Gangliosides are unusually abundant in the brain, but function as signal transduction regulatory molecules in many tissues where they are expressed in lower amounts (Allende and Proia 2014; Schnaar et al. 2014; Schnaar 2016). Among their functions, gangliosides regulate signaling by lateral association with receptor tyrosine kinases (Kaucic et al. 2006; Sonnino and Prinetti 2010), including the insulin receptor (IR) (Lipina and Hundal 2015), epidermal growth factor receptor (Liu et al. 2008), platelet-derived growth factor receptor (Mitsuda et al. 2002) and the TrkA high-affinity nerve growth factor receptor (Zakharova et al. 2014).

Gangliosides are synthesized stepwise (Figure 1) by a series of glycosyltransferases, some of which transfer sugars exclusively to glycolipid acceptors (Schnaar et al. 2014). Two of the 20 mammalian sialyltransferases, ST3Gal-II and ST3Gal-III, are responsible for adding the terminal sialic acid to 2 abundant gangliosides in mammals, GM1 and GD1b, to synthesize GD1a and GT1b, respectively (Sturgill et al. 2012). Genetic deletion of the gene that codes for ST3Gal-II (*St3gal2*) reduces GD1a/GT1b levels in the brain by about half, whereas knocking out the gene that codes for ST3Gal-III (*St3gal3*) has no significant effect on ganglioside biosynthesis. However, knocking out both *St3gal2* and *St3gal3* results in near total loss of GD1a and GT1b in the brain with commensurate increases in their precursors GM1 and GD1b. Notably, brain protein sialylation is quantitatively unchanged in *St3gal2*-null mice, but is decreased in *St3gal3*-null mice (Sturgill et al. 2012; Yoo et al. 2015). These data indicate that ST3Gal-II acts primarily or exclusively on glycosphingolipid acceptors. While studying *St3gal2*-null mice, we unexpectedly observed that older mice lacking the ST3Gal-II enzyme appeared obese. Since gangliosides have been reported to modulate IR signaling (Inokuchi 2014; Lipina and Hundal 2015), we initiated studies to document obesity and insulin resistance in *St3gal2*-null mice.

Results

St3gal2-null mice develop late-onset obesity

Mice lacking the enzyme ST3Gal-II (*St3gal2*-null mice) had a readily apparent age-dependent increase in body mass compared to wild type (WT) littermates when fed a regular chow diet (Figure 2A). Young adult (3-month-old) *St3gal2*-null mice were the same average weight as WT littermates (Figure 2B). However, the null mice steadily gained weight >50% faster (2.2 g/month) than their WT counterparts (1.4 g/month), resulting in a highly significant weight difference by 13 months of age. Upon sacrifice and dissection, all *St3gal2*-null mice had readily visible fat deposits in all organs (data not shown). Thirteen-month-old *St3gal2*-null and WT mice were scanned by quantitative nuclear magnetic resonance (QNMR) to determine fat, lean and water content. The results (Table I) revealed an increase of 50% in fat mass in *St3gal2*-null mice and of 9% in lean body mass with no change in water content. When the fat mass was normalized with lean mass, a significant increase of 37% ($P < 0.005$) in fat/lean weight ratio was observed in *St3gal2*-null mice compared to WT littermates. The data support the conclusion that *St3gal2*-null mice develop late-onset obesity.

St3gal2-null mice have late-onset hyperglycemia, reduced glucose clearance and insulin resistance

To test whether obesity in *St3gal2*-null mice is related to changes in insulin responsiveness, glucose clearance and insulin sensitivity were determined. At 9 months of age, *St3gal2*-null mice had fasting blood glucose levels that were 33% higher than their WT littermates ($P < 0.05$; Figure 3A). Younger *St3gal2*-null mice (3 month old) had a slightly higher average fasting blood glucose level than WT mice that was not statistically significant. Over the next 6 months, the

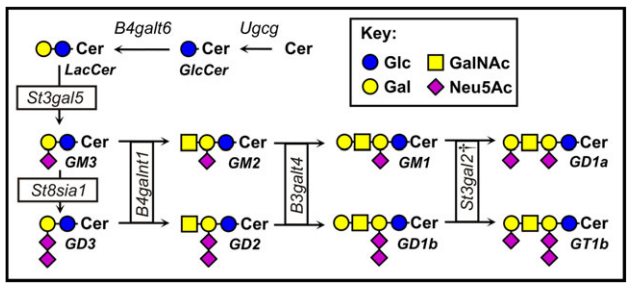

Fig. 1. Structures and biosynthetic pathways of major mammalian gangliosides. Symbols are according to Varki et al. (2015). †, in *St3gal2*-null mice terminal α2,3 sialylation of gangliosides GM1 and GD1b to produce GD1a and GT1b is partially compensated by the product of the *St3gal3* gene, ST3Gal-III (Sturgill et al. 2012). This figure is available in black and white in print and in color at Glycobiology online.

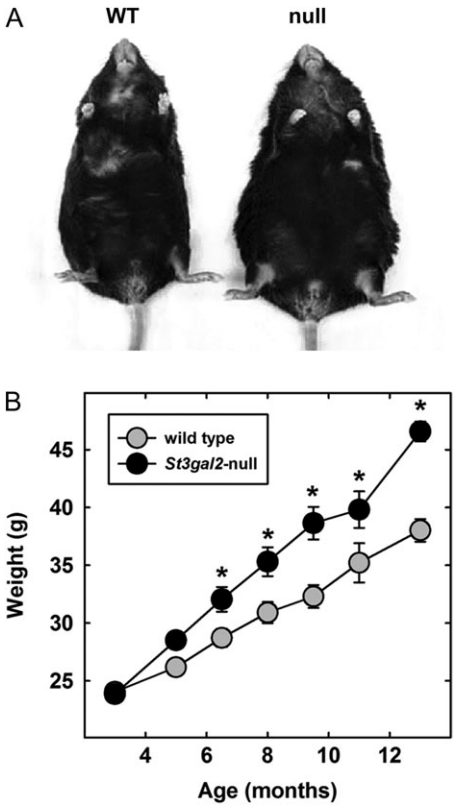

Fig. 2. *St3gal2*-null mice develop late-onset obesity. (**A**) Compared to their WT counterparts, 13-month-old *St3gal2*-null mice are visibly obese. (**B**) Developmental course of obesity in WT and *St3gal2*-null mice. Genotypes are significantly different by two-way analysis of variance (ANOVA) with $P < 0.001$. *$P < 0.01$ between genotypes by post-hoc Tukey analyses. $n = 6$–22 mice per group.

increase in fasting blood glucose was not significantly increased in WT mice but was significantly increased in *St3gal2*-null mice. Glucose tolerance tests revealed that 3-month-old *St3gal2*-null and WT mice had similar glucose tolerance curves, with a modest but significant decrease in clearance only at 15 min after glucose injection (Figure 3B). In contrast, 9-month-old *St3gal2*-null mice had significantly reduced glucose clearance compared to control over the entire time course measured.

Since prior studies reported that gangliosides can regulate IR sensitivity (Yamashita et al. 2003; Holland et al. 2007), insulin responsiveness was tested as a mechanism for hyperglycemia and obesity in *St3gal2*-null mice (Figure 4). Fasting serum insulin levels were not statistically different between *St3gal2*-null and WT mice, despite a trend toward higher levels in the null mice ($P = 0.064$, Figure 4A). However, blood glucose levels in 9-month-old *St3gal2*-null mice were significantly less responsive to intraperitoneal insulin injection compared to WT mice (Figure 4B). The initial insulin-induced drop in blood glucose in *St3gal2*-null mice is less than half that in WT mice. More notably, blood glucose levels continued to decrease in response to insulin in WT mice over the course of the 2-h experiment, whereas blood glucose levels in *St3gal2*-null mice quickly returned to pre-insulin levels by 60 min after insulin administration. These data are consistent with insulin resistance due to loss of ST3Gal-II.

Morphometric analyses of pancreatic sections revealed that St3gal2-null mice and their littermate WT controls had β-islets of the same area, aspect and general appearance (Figure 4C and data not shown).

To confirm insulin resistance at the molecular level and determine the potential tissue site(s) of insulin resistance, three major insulin target tissues, adipose tissue, liver and skeletal muscle, were collected from 9-month-old WT and *St3gal2*-null mice challenged with insulin (1 U/kg body weight) and insulin signaling studied by analysis of the phosphorylation levels of an upstream broadly distributed IR substrate, IR substrate 1 (IRS-1) and a downstream key intermediate in insulin-mediated metabolic control, the serine-threonine kinase Akt (Guo 2014; Saltiel 2016). Levels of phosphorylated IRS-1 were decreased nearly 68% and Akt-P by 49% in adipose tissue from *St3gal2*-null mice, whereas their levels were not decreased in skeletal muscle (Figure 5, Table II). Liver had a modest, 29% decrease in phosphorylated IRS-1 and no decrease in Akt-P. These data indicate deficits in insulin-induced molecular signaling in adipose tissue of *St3gal2*-null mice.

Table I. QNMR body mass and Oxymax metabolic profiles[a] of 13-month-old WT and *St3gal2*-null littermates

Metric	WT	*St3gal2*-null	Null/WT	*P*-value[b]
Weight (g)	37.6 ± 0.7	45.9 ± 1.0	1.22	<0.001
Fat mass (g)	12.8 ± 0.9	19.2 ± 0.5	1.50	<0.005
Lean mass (g)	22.6 ± 0.3	24.7 ± 0.7	1.09	<0.05
%fat	34.0 ± 1.9	41.9 ± 0.7	1.23	<0.005
Fat/lean ratio	0.57 ± 0.05	0.78 ± 0.02	1.37	<0.005
VO_2[c]	3000 ± 106	2560 ± 34	0.85	<0.005
VCO_2[c]	2960 ± 96	2450 ± 44	0.96	<0.001
RER	0.99 ± 0.01	0.96 ± 0.01	0.97	<0.02
EE[c]	15.1 ± 0.5	12.8 ± 0.2	0.85	<0.005
VO_2[d]	4970 ± 93	4760 ± 97	0.97	0.15
VCO_2[d]	4910 ± 66	4570 ± 109	0.97	<0.05
RER	0.99 ± 0.01	0.96 ± 0.01	0.97	<0.02
EE[d]	25.0 ± 0.4	23.8 ± 0.5	0.95	0.10

[a]VO_2, oxygen consumption rate (mL/kg/h); VCO_2, carbon dioxide production rate (mL/kg/h); RER, respiratory exchange ratio; EE, energy expenditure (kcal/kg/h).

[b]Student's t-test, n = 6 per genotype.

[c]Normalized to kg body weight.

[d]Normalized to kg lean weight.

St3gal2-null mice have altered adipose ganglioside expression

Because adipose tissue displayed altered insulin sensitivity in *St3gal2*-null mice compared to WT littermates, gangliosides were extracted from adipose tissues and analyzed by thin-layer chromatography (TLC, Figure 6) and mass spectrometry (MS) (Figures 7 and 8, Table III).

TLC analysis of WT adipose tissue revealed at least 16 resolved ganglioside species (Figure 6A), characteristic of gangliosides with different ceramide lipids as well as different glycans (Keranen 1976). Based on TLC migration and quantitative analyses of sialic acid staining, the major ganglioside of WT mouse adipose tissue was

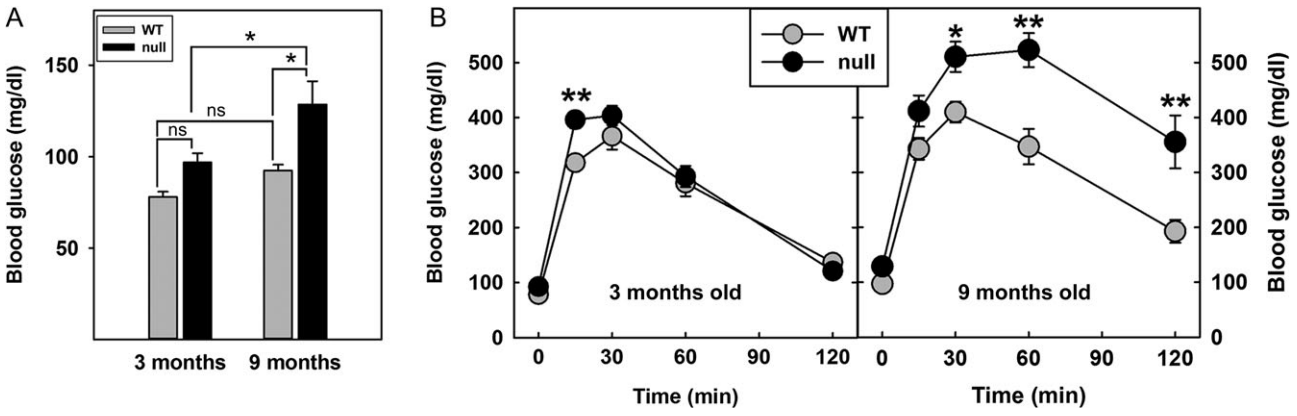

Fig. 3. *St3gal2*-null mice display age-related hyperglycemia and altered glucose clearance. (**A**) *St3gal2*-null mice (null) have increased blood glucose levels with respect to WT littermates at 9 months of age. Genotypes are significantly different by two-way ANOVA ($P < 0.05$). *$P < 0.05$, Tukey post-hoc analysis. $n = 6$–9 mice each group. (**B**) Glucose clearance was measured by peritoneal glucose solution administration ($t = 0$) with measurement of blood glucose for 2 h thereafter. Genotypes are significantly different by two-way ANOVA ($P < 0.02$ at 3 months, $P < 0.001$ at 9 months). *$P < 0.01$; **$P < 0.001$ by Tukey post-hoc analyses. Some values at 30–60 min for 9-month-old null mice reached the maximum of the analytical technique (600 mg/dL). Data are expressed as mean ± SE $n = 7$–9 mice per group.

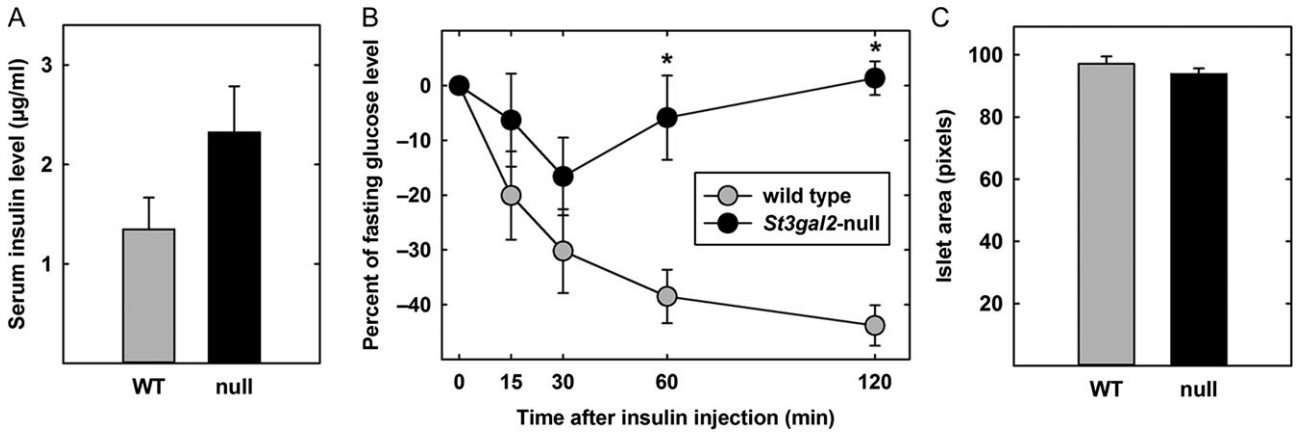

Fig. 4. *St3gal2*-null mice display marked insulin resistance. (**A**) Serum insulin levels are not significantly different between *St3gal2*-null (null) and WT mice. $P = 0.064$, $n = 15$–17 mice per group. (**B**) Insulin responses of WT and *St3gal2*-null mice. Insulin was injected intraperitoneally at $t = 0$ and blood glucose levels measured at indicated times up to 2 h thereafter. Values are expressed as percent difference from the value at $t = 0$. Genotypes are significantly different by two-way ANOVA ($P < 0.001$). *$P < 0.005$ by Tukey post-hoc analyses. $n = 5$–7 mice per group. (**C**) Morphometric analyses of β-islet size shows no significant difference between WT and *St3gal2*-null (null) mice ($P = 0.28$ by Student's *t*-test). $n = 3$ mice per group. Data are from pancreas cross sections (images not shown).

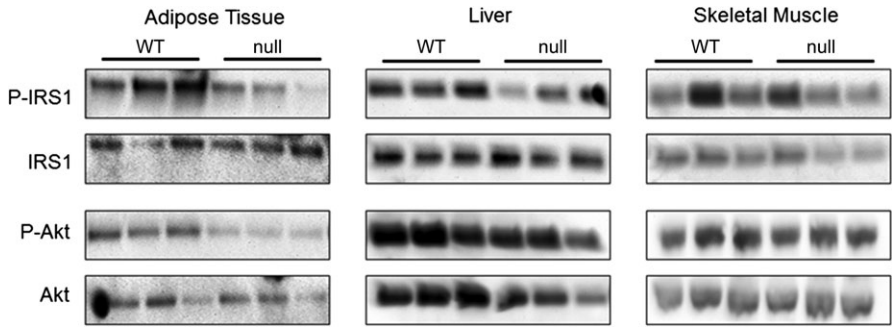

Fig. 5. Reduced phosphorylation of IR effectors IRS-1 and Akt in adipose tissue from *St3gal2*-null mice. Nine-month-old WT ($n = 3$) and *St3gal2*-null (null, $n = 3$) mice were treated with insulin (1 U/kg body weight) and then tissues were dissected, extracted and the extracted proteins were resolved by sodium dodecyl sulfate-polyacrylamide gel electrophoresis (SDS-PAGE). Resolved proteins were blotted to nitrocellulose membranes and immunoblotted with antibodies to phospho-IRS-1 (P-IRS-1), IRS-1 (IRS), phospho-Akt (P-Akt) and Akt. Images were scanned and quantitative results are reported in Table II.

Table II. Phosphorylation of IR effector proteins IRS-1 and Akt[a] in different tissues of 9-month-old WT and *St3gal2*-null mice

	Adipose		Liver		Skeletal muscle	
Genotype	IRS-P/IRS	Akt-P/Akt	IRS-P/IRS	Akt-P/Akt	IRS-P/IRS	Akt-P/Akt
WT	2.3 ± 0.9	1.8 ± 0.5	1.0 ± 0.1	0.9 ± 0.1	1.1 ± 0.2	1.4 ± 0.1
St3gal2-null	0.7 ± 0.3	0.9 ± 0.1	0.7 ± 0.2	1.2 ± 0.1	1.2 ± 0.1	1.5 ± 0.1
Null/WT ratio	0.32	0.51	0.71	1.2	1.1	1.0

[a]Pixel intensities of bands on images of immunoblots were analyzed using ImageJ and total density per band determined. Values for phosphoproteins (arbitrary units) were divided by values for total proteins of each type and are reported as ratios.

GM3 with significant amounts of GM2, GM1, GD1 (GD1a and/or GD1b) and GT1b. *St3gal2*-null adipose tissue had reduced GM3 expression, increased GM1 expression (confirmed using TLC immuno-overlay with anti-GM1 monoclonal antibody, data not shown), and an absence of GT1b (Figure 6B). Although TLC staining of GD1 species was equivalent between WT and *St3gal2*-null mice, distinguishing between GD1a and GD1b was not possible using this technique due to heterogeneity of ceramide species and overlapping migration with standards. However, TLC immuno-overlay (using anti-GD1a monoclonal antibody) revealed a 67% decrease in GD1a in *St3gal2*-null mice compared to WT (data not shown). GD3 (which migrates near GM1) was not quantitatively significant by MS analyses (see below).

MS of permethylated gangliosides was consistent with the TLC data, and revealed significant differences in *St3gal2*-null mouse adipose tissue ganglioside expression compared to that in WT mice (Figures 7 and 8). GM3 was the major ganglioside species in WT mice, with a remarkable 27 distinct species of GM3 identified based on different sialic acid *N*-acyl groups (*N*-acetyl (Neu5Ac) or *N*-glycolyl (Neu5Gc)) and ceramide lipid variations. WT mice expressed more GM3 (and different GM3 species, Table III), whereas *St3gal2*-null mice expressed more GM1. Masses for GD3 were not detected

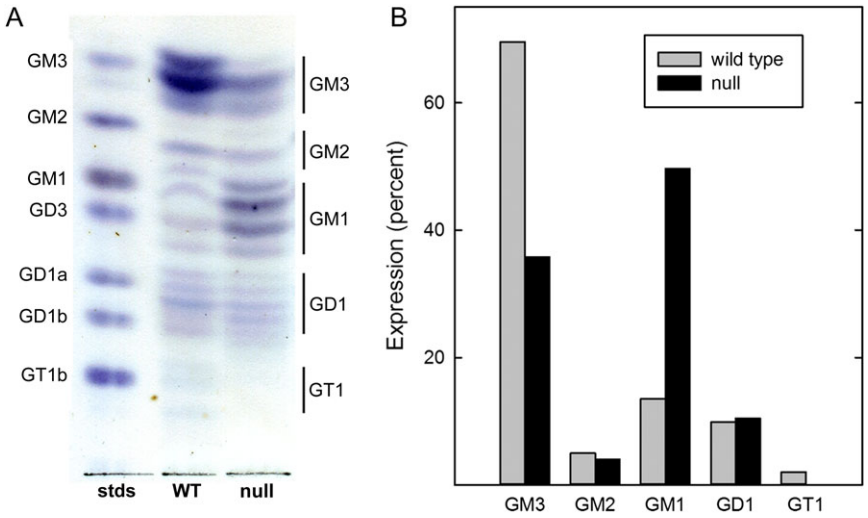

Fig. 6. Altered ganglioside expression in adipose tissue from *St3gal2*-null mice. (**A**) Gangliosides from visceral adipose tissue from adult WT and *St3gal2*-null (null) mice (11 months old) were extracted, partially purified, subjected to silica gel TLC and stained with the sialic acid-specific resorcinol reagent. Samples were loaded at equivalent weights of adipose tissue. Ganglioside standards are identified at the left and adipose ganglioside assignments (based on migration and immuno-overlay) to the right. The image was uniformly contrast enhanced for presentation. (**B**) Images of stained TLC plates (not contrast enhanced) were subjected to quantitative image analysis using ImageJ software. Relative staining densities were adjusted for the number of sialic acids in each species and are expressed as percent of total gangliosides. This figure is available in black and white in print and in color at Glycobiology online.

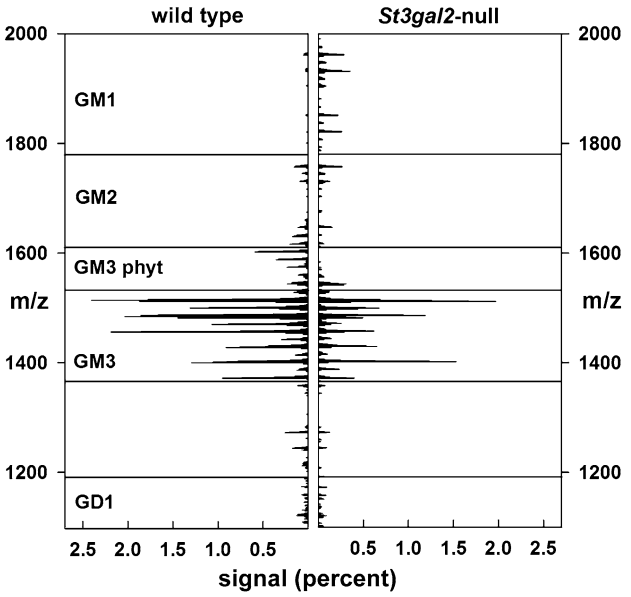

Fig. 7. Total ion mapping MS of gangliosides extracted from WT and *St3gal2*-null mouse adipose tissues as described in the text and legend to Figure 6. Signal intensities are expressed as a percent of total ganglioside-related signals.

in either sample, and higher order gangliosides were either very minor (GD1) or absent (GT1b) in the MS-processed samples. Quantitative analyses (Figure 8, Table III) revealed that, as in the TLC analyses, *St3gal2*-null mouse adipose tissue had relatively less GM3 and more GM1 expression. The GM3 Neu5Ac:Neu5Gc ratio was the same between null and WT mice, whereas the amount of hydroxy fatty acid in GM3 ceramide was relatively higher in *St3gal2*-null mice (Figure 8). Ceramide heterogeneity was much less in GM1 species, with only three fatty acids (C16:0, C24:1 and C24:0) predominating (data not shown). Total GM1 levels were >10-fold higher in *St3gal2*-null mice, with an increase in the Neu5Ac:Neu5Gc ratio and no difference in relative fatty acid hydroxylation (Figure 8).

Total glycoprotein sialic acid was quantitatively unchanged in *St3gal2*-null mouse adipose tissue (104% ± 11% compared to WT mice, $n = 3$ of each genotype).

Insulin-induced phosphorylation of Akt in mouse 3T3-L1 adipocytes is increased by preincubation with exogenous GM3 or GT1b, but not GM1

Ganglioside analyses (Figure 6) indicate increased GM1 with decreased GT1b and GM3 in *St3gal2*-null adipose compared to WT mouse adipose. To test whether these gangliosides alter insulin signaling when added exogenously, each was added to mouse 3T3-L1 adipocytes for 24 h prior to testing cellular insulin responses. Whereas exogenous GM1 had no effect on insulin-induced Akt phosphorylation (Figure 9), surprisingly both GT1b and GM3 significantly increased insulin signaling.

St3gal2-null mice have reduced energy metabolism and increased locomotor activity

Indirect calorimetry was used to characterize metabolic changes contributing to obesity in *St3gal2*-null mice (Table I). Compared to WT littermates, *St3gal2*-null mice displayed a reduction in rates of oxygen consumption normalized to body weight. Similar percent decreases were found during light and dark periods (comparison data not shown). The respiratory exchange ratio (RER) was also significantly decreased in *St3gal2*-null mice compared to WT mice, suggesting an increase in β-oxidation of lipids as their source of energy. There was no significant difference in the RER during the light (rest) cycle (0.96, WT and null mice), but *St3gal2*-null mice showed a marked reduction in RER during the dark (active) cycle (1.01 for WT; 0.95 for null mice, $P < 0.0005$). Compared to WT littermates, *St3gal2*-null mice also displayed a reduction in energy expenditure

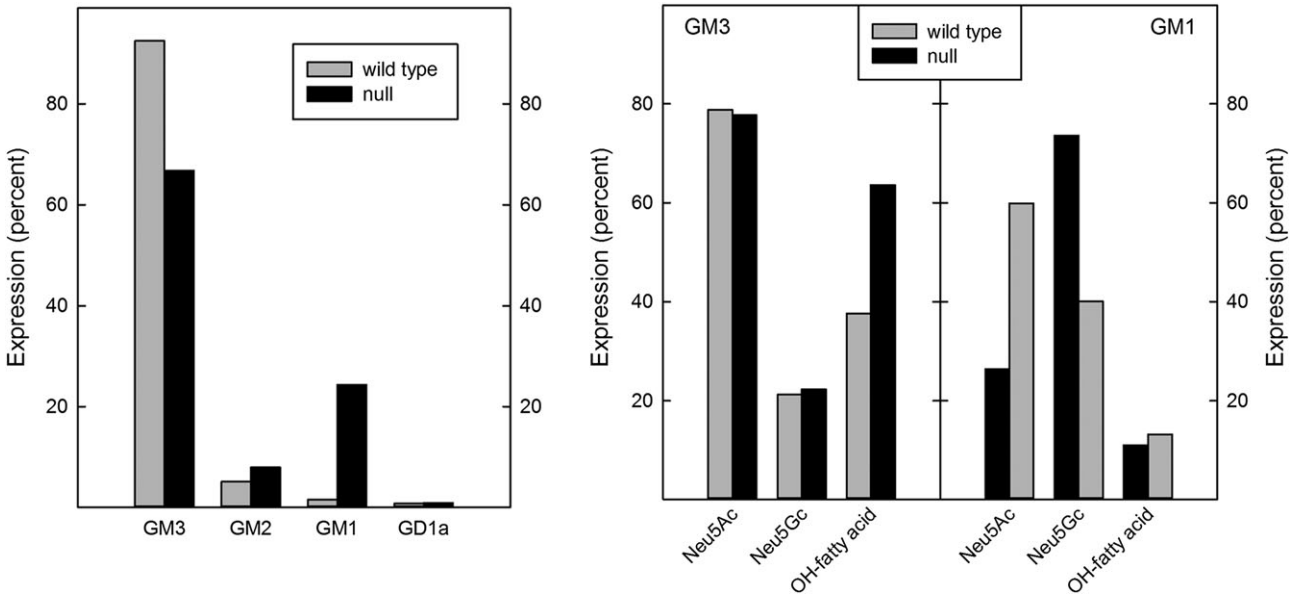

Fig. 8. Comparative ganglioside expression in WT and *St3gal2*-null mice. The summed MS signal (see Fig. 7) for each ganglioside species detected (left panel) are expressed a percent of total ganglioside signals. Within the species of GM3 (Table III) and GM1 detected, the percent expression of Neu5Ac vs. Neu5Gc as well as percent of total gangliosides with hydroxy fatty acids are shown (right panel).

Table III. GM3 structures in adult WT and *St3gal2*-null mouse (11 months old) adipose tissues[a]

Fatty acid	WT			*St3gal2*-null		
	Neu5Ac		Neu5Gc	Neu5Ac		Neu5Gc
	NH-FA (%)	OH-FA (%)	NH-FA (%)[b]	NH-FA (%)	OH-FA (%)	NH-FA (%)[b]
C16:0	4.8	3.2	3.0	2.9	13.8	6.0
C18:0	5.3	1.7	0.8	0.8	4.8	1.5
C20:0	3.6	2.2	0.3	0.8	5.1	1.2
C22:0	8.8	8.1	2.5	1.1	8.6	1.7
C23:1		0.9	0.6		2.9	1.0
C23:0	5.1	4.9	2.1		4.5	1.2
C24:1	5.9	3.5	5.2	3.7	14.1	4.7
C24:0	7.7	6.0	5.9	2.3	7.7	3.3
C24:0 phyt					0.5	0.3
C24:1 phyt					1.0	1.1
C26:1						
C27:0					0.3	
C26:0 phyt	0.8	1.0		2.7		
C27:0 phyt		1.9				
C28:0 phyt		3.4				
TOTALS	41.9	36.8	20.5	14.4	63.3	22.0

[a]Fatty acid assignments (NH-FA, nonhydroxy fatty acids; OH-FA, hydroxy fatty acids) are based on mass assuming d18:1 sphingosine. MS^2 data were used to determine Neu5Ac:Neu5Gc ratios for masses indicating a single extra hydroxy group, which was assigned to Neu5Gc or the fatty acid. phyt = species with masses consistent with phytosphingosine as the ceramide base.

[b]Less than 1% of GM3 species (0.8% WT, 0.3% *St3gal2*-null) was found as Neu5Gc-GM3 with hydroxy fatty acids (data not shown).

(EE) normalized to body weight. *St3gal2*-null mice did not have increased food intake (g/d, 5.3 ± 0.2 for WT; 5.4 ± 0.1 for nulls), ruling out hyperphagia as a significant contributing factor to the obesity. It is notable that while RER differences were significant when data were normalized to body weight or lean weight, the reduction in oxygen consumption in *St3gal2*-null mice was only significant when normalized to body weight (Table I), results consistent with selectively altered adipose metabolism.

To test whether reduced locomotor activity contributed to obesity in *St3gal2*-null mice, open-field activity was measured over a 24-h period using automated photometric cages. Far from being lethargic, the *St3gal2*-null mice had increased locomotor activity during the active (dark) cycle (Figure 10). These results are consistent with increased locomotor activity reported in *B4galnt1*-null mice (Pan et al. 2005), which have a block in ganglioside metabolism upstream of ST3Gal-II activity (see Figure 1). Considered together, metabolic

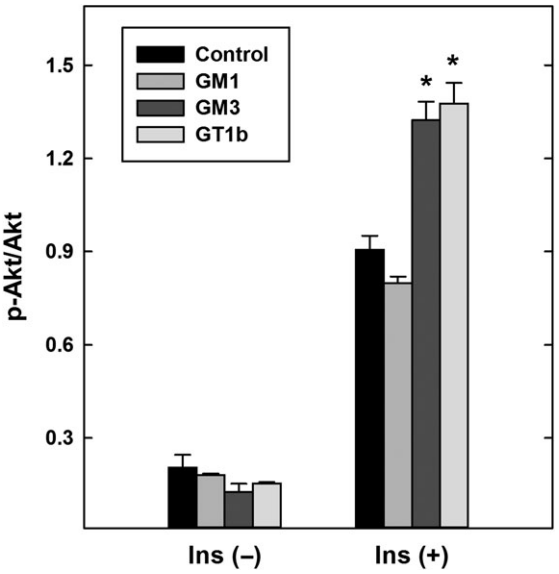

Fig. 9. Exogenous addition of gangliosides GM3 and GT1b (but not GM1) to 3T3-L1 adipocytes enhances insulin-mediated Akt phosphorylation. Adipocyte-differentiated 3T3-L1 cells were cultured for 24 h in medium containing 50 μM BSA (control) or 50 μM ganglioside–BSA complex as indicated. After washing, cells were treated for 5 min with 10 nM insulin, lysed, and the relative amount of phosphorylated Akt compared to total Akt was determined by immunoblotting. Data are expressed as the ratio of arbitrary density units. Cells treated with GM3 or GT1b (but not GM1) had a higher relative phospho-Akt than WT ($P < 0.001$, two-way ANOVA). *$P < 0.001$, Tukey post-hoc analyses. Data are expressed as mean ± SE $n = 3$ replicate cultures per group. BSA, bovine serum albumin.

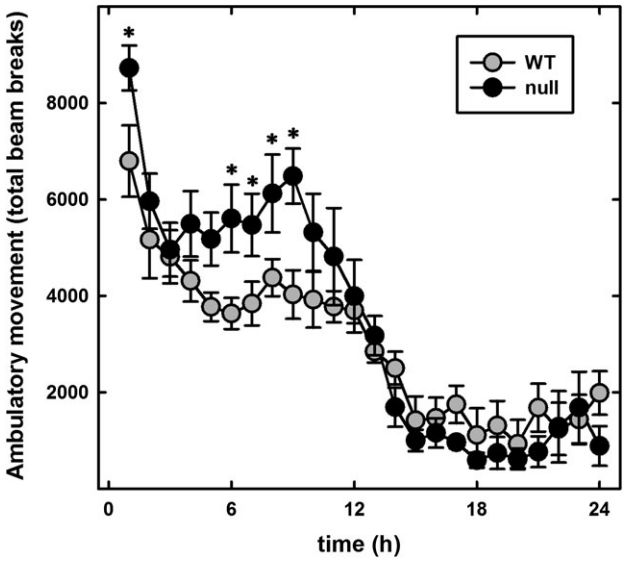

Fig. 10. *St3gal2*-null mice display increased locomotor activity. Open-field activity of 6-month-old WT and *St3gal2*-null (null) mice was automatically quantified over a 24-h period using photometric beams. The first 12 h represents the dark cycle and the last 12 h the light cycle. Null mice were significantly more active than WT ($P < 0.005$, two-way ANOVA). *$P < 0.05$, Tukey post-hoc analyses. Data are expressed as mean ± SE $n = 6$ mice per group.

and open-field activity data are consistent with altered metabolic regulation rather than altered mobility contributing to obesity in *St3gal2*-null mice.

Discussion

Mice lacking the enzyme ST3Gal-II exhibit insulin resistance and obesity. ST3Gal-II is highly selective for adding α2,3-sialic acid to the terminal galactose of the acceptor disaccharide Galβ1-3 GalNAc, with very low activity for Galβ1-3GlcNAc and none for Galβ1-4GlcNAc (Tsuji and Takashima 2014). The preferred Galβ1-3GalNAc acceptor determinant is abundant as the terminus on the major gangliosides GM1 and GD1b, which are converted by ST3Gal-II to GD1a and GT1b, respectively (Sturgill et al. 2012). Although the same acceptor disaccharide is found on O-linked glycoproteins (the T-antigen), kinetic studies indicate that gangliosides are the predominant acceptors for ST3Gal-II, whereas O-linked glycoproteins are better acceptors for ST3Gal-I (Tsuji and Takashima 2014). Furthermore, data from brain (Sturgill et al. 2012; Yoo et al. 2015) and adipose (this article) indicate that total glycoprotein sialylation is quantitatively unchanged in tissues of *St3gal2*-null mice. Although it is possible that some O-linked glycoprotein glycans are altered in these *St3gal2*-null mice, the simplest hypothesis consistent with these data is that changes in adipose ganglioside (glycosphingolipid) sialylation are responsible for an insulin-resistant phenotype.

Multiple lines of evidence indicate that the simple ganglioside GM3 (see Figure 1) regulates IR sensitivity via direct lateral interactions with the IR in the plane of the membrane (Inokuchi 2014; Lipina and Hundal 2015). Those data support a model in which GM3-IR interactions sequester the IR from caveolae, inhibiting IR-mediated signaling (Kabayama et al. 2007). Increasing GM3 synthesis by treatment with TNF-α suppresses IR signaling, with the TNF-α effect pharmacologically reversed by blocking GM3 biosynthesis (Tagami et al. 2002). In vivo, evidence supporting GM3 as a regulator of insulin sensitivity comes from mice genetically engineered to lack GM3 (Yamashita et al. 2003). Although GM3-deficient mice (*St3gal5*-null) were viable and without major abnormalities, they displayed enhanced IR phosphorylation and were protected from high-fat diet-induced insulin resistance (Yamashita et al. 2003; Nagafuku et al. 2015). Consistent with these findings, pharmacological inhibition of glycosphingolipid biosynthesis at the level of glucosylceramide enhances insulin sensitivity in vitro (Kabayama et al. 2007) and in vivo (Aerts et al. 2007; Zhao et al. 2007; van Eijk et al. 2009; Yew et al. 2010). Together, these data support the conclusion that ganglioside GM3, in particular, down-regulates IR sensitivity.

Exogenous addition of gangliosides to intact cultured cells has the potential to result in membrane insertion. Prior studies adding gangliosides to mouse 3T3 adipocytes in culture revealed that GM3 (100 μM) but not GD1a reduced insulin-mediated IR self-phosphorylation and to a lesser extent IRS-1 phosphorylation (Tagami et al. 2002). In this study, using 50 μM exogenous ganglioside complexed with fatty acid-free BSA, GM1 had no effect, whereas GM3 (and GT1b) increased IRS-1 and Akt phosphorylation. The difference in the outcome of GM3 exogenous addition in this study may relate to the source of GM3, which was from bovine milk in the prior study and from canine blood in this study. Differences in ceramide structures, notably in fatty acid chain lengths, may account for different biological effects (or pharmacological effects of endogenously added gangliosides). The highly varied GM3 ceramide structures found in mouse adipose tissues in this study invite the hypothesis that diverse GM3 lipid structures may drive diverse molecular interactions. Prior studies on ganglioside-mediated regulation of

tyrosine kinase receptors have addressed differential effects of the same ganglioside on the same receptor system depending on cell type, ganglioside species (both carbohydrate and lipid) and experimental conditions (Kaucic et al. 2006).

The published evidence of gangliosides other than GM3 in regulating insulin sensitivity is less clear. Insulin-induced autophosphorylation of solubilized and partially purified IR's from lymphoblast cells or skeletal muscle is reduced by addition of several gangliosides to the receptor phosphorylation assays, including GM3, GM2, GM1, GD1a and GT1b (Nojiri et al. 1991; Sasaki et al. 2003). Recently, increased ganglioside GM1 was associated with reduced insulin sensitivity in late-passage (senescent) human endothelial cells in culture (Sasaki et al. 2015). However, genetic evidence for the roles of gangliosides other than GM3 in regulating the IR has been limited. Data from this study are consistent with the hypothesis that a shift from higher gangliosides (GD1a, GT1b) to GM1 in adipose tissue contributes to insulin resistance, and that *St3gal2*-null mice are a genetic model of late-onset diabetes. Changes in GM3 molecular species, which were also found, may be an outcome or a contributing factor to obesity. The notable shift toward hydroxy fatty acids in the ceramide of GM3 from *St3gal2*-null mice is notable in light of recent data demonstrating differential enhancement of GM3 fatty acid hydroxylation in humans with metabolic syndrome (Veillon et al. 2015). The question of whether these changes are an outcome or cause of obesity in both mice and humans is worthy of further investigation. Genetic alteration of fatty acid chain length in sphingolipids (including but not exclusively gangliosides) is associated with insulin resistance in liver but not adipose, indicating yet another level of sphingolipid control of insulin sensitivity (Park et al. 2013).

Loss of ST3Gal-II resulted in impaired whole-body insulin sensitivity, as indicated by a reduced glucose shift into peripheral tissues in response to either glucose or insulin challenges. This study demonstrates insulin resistance, as measured by decreased insulin-mediated substrate and downstream target phosphorylation, primarily in adipose tissue. Consistent with this finding, mouse adipose tissue expresses complex gangliosides including GM1, GD1a, GD1b and GT1b (Figure 6 and Ohashi 1979). A reasonable hypothesis consistent with these data is that increased GM1 and/or decreased GD1a and GT1b is/are responsible for impaired insulin action in *St3gal2*-null mice. In this light, the ability to exogenous GT1b but not GM1 to enhance insulin-mediated insulin signaling (Figure 9) may be relevant. Compared to mouse adipose, mouse liver and muscle have little or no GM1 or higher gangliosides (Sasaki et al. 2003), consistent with the relative lack of altered insulin-stimulated signaling in these tissues in *St3gal2*-null mice. By comparison, transgenic mice overexpressing the ganglioside sialidase gene *NEU3* in all tissues developed a diabetic phenotype, whereas selective overexpression of *NEU3* in liver had the opposite effect (Sasaki et al. 2003; Lipina et al. 2015). These data may be explained by considering the substrates of Neu3 sialidase. GM3 is eliminated by Neu3, whereas gangliosides GD1a, GD1b and GT1b are converted to GM1 (GM1 and GM2 are resistant to this sialidase) which may induce insulin resistance. In tissues expressing primarily GM3, Neu3 may increase insulin sensitivity, whereas in tissues with GD1a and GT1b, conversion to GM1 may result in insulin resistance. Therefore, the effects of Neu3 sialidase would be tissue-specific.

The obese phenotype in *St3gal2*-null mice was late-onset, with mice showing a significant increase in body weight at 5 months. Nevertheless, *St3gal2*-null mice displayed mildly but significantly reduced clearance of blood glucose at 3 months of age, before a significant increase in body weight was apparent, suggesting that insulin resistance preceded obesity. Poor glucose clearance in these mice was attributed, at least in part, to reduced IR sensitivity as judged by their impaired signaling in response to exogenous insulin. Our conclusion is that a shift in complex ganglioside levels in adipose (increased GM1, decreased GD1a and GT1b) results in insulin resistance, and that *St3gal2*-null mice display a late-onset obese diabetic phenotype. Although the causative role (if any) of ganglioside shifts in the etiology of diabetes is unknown, it may be relevant that adipose tissue from diet-induced obese insulin-resistant mice have increased complex gangliosides including GM2, GM1 and GD1a (Tanabe et al. 2009). Given these observations, the relationships between obesity, diabetes and ganglioside expression patterns in adipose tissue are worth further consideration.

Materials and methods

Mice

St3gal2-null mice were produced by targeted gene disruption as described previously (Ellies et al. 2002). Genotypes were determined using polymerase chain reaction (PCR) with oligonucleotide primers 5′-CTTTGCGACAGGGTTTCATT and 5′-CAGGGTT GCTCAACAAGTG. Alternatively, genotyping was outsourced for determination by real time PCR (Transnetyx, Cordova, TN). Mice were routinely maintained in a 14-h light/10-h dark cycle and fed with standard mouse chow (Harlan Teklad 2018SX, Harlan Laboratories, Indianapolis, IN). All procedures were approved by Institutional Animal Care and Use Committees and were consistent with federal law and National Institutes of Health (NIH) regulations.

Ganglioside and sialoglycoprotein analyses

Gangliosides were extracted and quantified as previously reported (Schnaar 1994). Briefly, 0.4–1.3 g of visceral adipose was homogenized on ice in 10 volumes of water (W) using a Potter-Elvehjem homogenizer. At ambient temperature, methanol (M) and then chloroform (C) were added to give a ratio of C–M–W (4:8:3). After thorough mixing, insoluble material was removed by centrifugation (1250 × *g*, 15 min), the supernatant collected and the pellet saved for sialoglycoprotein determination. The supernatant was loaded onto a 3-mL column of DEAE-Sepharose (acetate form), the column washed with C–M–W (4:8:3) and methanol, and gangliosides eluted with 200 mM ammonium acetate in methanol. The eluate was evaporated under a stream of nitrogen and treated with 2 mL of 0.5 M NaOH in methanol at 60°C for 2 h. Samples were cooled, neutralized with 0.5 M acetic acid, adjusted by solvent addition to C–M–W (2:43:55) and loaded onto a tC18 Sep-Pak cartridge (Waters, Milford, MA). The cartridge was washed with the same solvent mixture, methanol–water (1:1) and then gangliosides eluted with methanol. The eluate was evaporated under vacuum and redissolved in methanol at 50 µL per gram of original tissue for analyses.

Aliquots were subjected to silica gel TLC using chloroform–methanol–0.25% aqueous KCl (60:35:8) as developing solvent. Gangliosides were visualized using a quantitative sialic acid-specific colorimetric resorcinol reagent (Schnaar and Needham 1994). The plates were scanned and resorcinol-stained spots quantified using ImageJ (Research Services Branch, National Institute of Mental Health). Alternatively, gangliosides GM1 and GD1a were detected after TLC resolution by immuno-overlay using anti-ganglioside antibodies as described (Lopez and Schnaar 2006).

For MS analysis, dried ganglioside samples were further purified by washing with *n*-hexane. The purified gangliosides were

permethylated as described (Anumula and Taylor 1992). The permethylated gangliosides were further purified by dissolving in 50% methanol and loading onto a water-prewashed tC18 Sep-Pak cartridge and permethylated gangliosides eluted with pure methanol. Maltotri- and tetra-saccharides were permethylated with ^{13}C-methyl iodine as internal standards.

Permethylated gangliosides were reconstituted in 50 μL of methanol/2-propanol/1-propanol/water (16:3:3:2 by volume) containing 1 mM NaOH for infusion. Ten picomole of maltooligosaccharide standards were spiked into each glycosphingolipid sample and the mixture was analyzed by infusion into a linear ion trap mass spectrometer (LTQ; ThermoFisher Scientific, Waltham, MA) using a nanoelectrospray source at a syringe flow rate of 0.40–0.60 μL/min and capillary temperature set to 210°C (Anumula and Taylor 1992; Vukelic et al. 2005; Aoki et al. 2007; Nimrichter et al. 2008). The instrument was tuned with a mixture of permethylated glycosphingolipid standards for positive ion mode. For fragmentation by collision-induced dissociation (CID) in MS/MS and MS^n, a normalized collision energy of 35–40% was used.

Detection and absolute quantification of the prevalence of individual gangliosides was accomplished using the total ion mapping and neutral loss scan functionality of the Xcalibur software package version 2.0 (ThermoFisher Scientific) as previously described (Aoki et al. 2007). Briefly, for total ion mapping, the *m/z* range from 600 to 2000 was automatically scanned in successive 2.8 mass unit windows with a window-to-window overlap of 0.8 mass units, which allowed the naturally occurring isotopes of each glycolipid species to be summed into a single response, thereby increasing detection sensitivity. Gangliosides were identified as singly (monosialo) or doubly charged (disialo), sodiated species in positive mode. For neutral loss scans, an MS workflow was defined in which the highest intensity peak detected by full MS was subjected to CID fragmentation. Preliminary analysis demonstrated that the major fragment ions in CID MS/MS scans of glycosphingolipid preparations correspond to the neutral loss of the ceramide moiety, leaving intact glycosphingolipid oligosaccharide ions. Therefore, the neutral loss scan workflow was set to acquire MSn fragmentation if an MS/MS profile contained an ion with *m/z* equivalent to loss of the most prevalent ceramide moiety. Following this data-dependent acquisition, the workflow returned to the full MS, excluded the parent ion just fragmented and chose the peak of next highest intensity for the same MS/MS and MS^n analysis. By this data-dependent acquisition workflow, glycosphingolipid glycan profiles and MS^n sequencing were rapidly acquired for complex mixtures.

Fatty acid assignments were based on mass assuming d18:1 sphingosine. MS^2 data were used to determine Neu5Ac:Neu5Gc ratios for every ganglioside mass. For every mass containing an extra permethylated hydroxy group, each was assigned to either Neu5Gc or the fatty acid depending on the predetermined Neu5Ac:Neu5Gc ratio. Signal assignments for overlapping monoisotopic peaks (e.g. the same ganglioside with C24:1 and C24:0 fatty acids) were arbitrarily assigned to the higher mass partner.

For glycoprotein sialic acid determinations, the methanol–chloroform–water precipitate containing the cellular proteins (see above) was dried at ambient temperature, then was fully solubilized in 0.1 M aqueous NaOH. Aliquots of solubilized brain protein were neutralized with HCl, then dissolved in 0.1 M HCl, 0.25 M NaCl and heated at 80°C for 3 h. Aliquots of the acid hydrolysates were analyzed for sialic acid using Dionex strong anion exchange high-performance liquid chromatography coupled with pulsed amperometric detection as described previously (Rohrer 2000). Aliquots of standard sialic acid of known concentration were hydrolyzed in parallel to correct for recovery.

Glucose tolerance, insulin responsiveness and insulin levels

Glucose tolerance was determined in *St3gal2*-null mice and age-matched WT littermate controls ($n = 8$ each group). Mice were fasted for 15 h prior to testing. On the day of the test, mice were weighed and their fasting blood glucose level was measured on freshly collected tail vein blood using an ACCU-CHEK Aviva blood glucose meter (Roche Diagnostics, Indianapolis, IN) with a detection range of 20–600 mg/dL (detection based on glucose oxidase reaction). Mice were then injected intraperitoneally with 2 g/kg body weight of D-glucose as a 20% saline solution and tail vein blood glucose levels were determined 15, 30, 60 and 120 min thereafter.

Insulin responsiveness was determined after measurement of fasting blood glucose (as above). Mice were injected intraperitoneally with 0.75 U/kg body weight of diluted Regular Human Insulin (HumulinR, Eli Lilly and Company, Indianapolis, IN) and blood glucose levels were determined (as above) 15, 30, 60 and 120 min thereafter.

Serum insulin levels were determined using tail vein blood of 9-month-old mice ($n = 10$ per group) that had been fasted for 15 h. Sera were separated and stored at −70°C prior to testing. Serum insulin levels were determined with an Ultrasensitive Mouse Insulin ELISA kit (Mercodia AB, Uppsala, Sweden) according to the manufacturer's instructions.

Phosphorylation of IR effectors

For insulin signaling analyses, 9-month-old *St3gal2*-null and WT littermates were fasted for 15 h before being given an intraperitoneal injection of insulin (1 U/kg body weight). Adipose, liver and soleus muscle were then dissected and homogenized immediately in ice-cold Tissue Protein Extraction Reagent (ThermoFisher) supplemented with protease inhibitors (Roche Applied Science, Indianapolis, IN) and phosphatase inhibitors (Sigma-Aldrich, St. Louis, MO). The protein content of the supernatant was determined using the Pierce BCA protein assay kit (ThermoFisher). Equal protein amounts of each sample were boiled for 4 min at 100°C after the addition of an equal amount of 2× SDS loading buffer. The proteins were separated by electrophoresis (NuPAGE 10% or 4–12% BisTris gel, Invitrogen) according to the manufacturer's instructions. The gels were blotted onto nitrocellulose membranes (Bio-Rad, Hercules, CA) and stained with Ponceau S red (Sigma-Aldrich) to confirm equal loading and transferring of proteins to the membrane in each lane. Immunoblotting was performed using antibodies that recognize phospho-Akt (Thr-308), Akt (loading control) and IRS-1 (loading control) from Cell Signaling (Danvers, MA) and phospho-IRS-1 (Tyr-612) from BIOSOURCE International (Camarillo, CA). Secondary antibodies were conjugated to horseradish peroxidase, and the signals were developed by chemiluminescence (GE Healthcare, Pittsburgh, PA). The signals were imaged using FluorChem Q multiImage III (AlphaInnotech, San Leandro, CA) and quantified as phospho-Akt/Akt and phospho-IRS-1/IRS-1 ratios using ImageJ software.

Insulin-stimulated Akt phosphorylation in ganglioside-treated 3T3-L1 adipocytes

Mouse 3T3-L1 cells were cultured in maintenance medium composed of Dulbecco's Modified Eagle Medium (DMEM, Invitrogen) supplemented with 10% fetal bovine serum and penicillin/streptomycin

(ThermoFisher). Two days after cells reached confluency, adipocyte differentiation was induced with DMEM supplemented with 0.5 mM methylisobutylxanthine (IBMX), 1 µM dexamethasone and 4 µg/mL insulin for 3 d and 4 µg/mL insulin for an additional 2 d. Cells were then returned to maintenance medium for 3 d by which time >90% of the cells differentiated into mature adipocytes laden with lipid droplets.

Gangliosides (750 nmol each of canine blood GM3 from Sigma-Aldrich and bovine brain GM1 and GT1b from Matreya, State College, PA) were dissolved in 1 mL of DMEM containing 750 nmol (49.5 mg) of fatty acid-free BSA (Sigma-Aldrich). After gangliosides were dissolved, each solution was diluted to 15 mL (50 µM ganglioside–BSA) with serum-free DMEM. Adipocytes were treated with vehicle control (50 µM BSA) or 50 µM ganglioside–BSA mixtures in DMEM for 24 h. After washing with PBS, cells were treated with (or without) 10 nM insulin for 5 min, lysed using 20 mM Tris-HCl, 150 mM NaCl, 1 mM EDTA, 0.5% NP-40 and 10% glycerol, and lysates subjected to immunoblot analyses (as described under "Phosphorylation of IR effectors") using anti-Phospho-Akt (Ser473) and anti-Akt (loading control) antibodies (Cell Signaling). Band intensities on immunoblots were quantified using ImageJ software.

Body composition and calorimetry

Total body fat, lean mass and total body water were determined in *St3gal2*-null mice and WT littermate controls ($n = 6$ per group) by QNMR using an Echo-MRI-100^{TM} Analyzer system (Echo Medical Systems, Houston, TX). These studies were performed at the Johns Hopkins University Phenotyping Core.

Indirect calorimetry was conducted using an open-flow indirect calorimeter (Oxymax Equal Flow System; Columbus Instruments, Columbus, OH) at The Johns Hopkins Center for Metabolism and Obesity Research. Mice were acclimated to the test facility for 1 week, monitored during acclimation to calorimetry chambers for 3 d and then monitored for a fourth day. Daily body weights and chow intakes (corrected for spillage) were measured to confirm acclimation. Rates of oxygen consumption (VO_2, mL/kg/h) and carbon dioxide production (VCO_2, mL/kg/h) were recorded for each chamber every 17 min. RER (VCO_2/VO_2) and rates of EE were calculated by Oxymax software (v. 4.02). EE was calculated using the formula $EE = CV \times VO_2$, in which CV is the caloric value, derived from the RER and constants from the table of Lusk (1928) ($CV = 3.815 + (1.232 \times RER)$). Average values for VO_2, RER and EE were calculated per subject for 24 h, and for the corresponding 12-h dark and 12-h light periods. Data were analyzed by unpaired, two-tailed Student's *t*-test.

Morphometric analyses

St3gal2-null mice and WT littermates ($n = 3$ each group) were transcardially perfused with saline then 4% paraformaldehyde in saline. The pancreas was harvested and further fixed in 4% paraformaldehyde for 24 h. Five semi-serial 10-µm plastic embedded sections from each pancreas were stained with hematoxylin-eosin to visualize pancreatic β-islets. Images comprising the entire length of the pancreas were acquired using a Nikon TE300 microscope fitted with a Photometrics CoolSNAP HQ2 camera (Roper Scientific, Duluth, GA). Morphometric studies were performed using NIS Elements software (Nikon). Data were analyzed by Student's *t*-test.

Locomotor activity

St3gal2-null and WT littermates ($n = 6$ each group) were placed in photobeam activity open-field chambers (San Diego Instruments, San Diego, CA). Two levels of photobeams measured locomotor and rearing activities in a test arena that was 15″ (width) × 15″ (depth) × 12″ (height).

Funding

National Institutes of Health grants NS037096 (R.L.S) and DK084171 (G.W.W).

Conflict of interest

None declared.

Abbreviations

ANOVA, analysis of variance; EE, energy expenditure; IR, insulin receptor; IRS, insulin receptor substrate; NIH, National Institutes of Health; QNMR, quantitative nuclear magnetic resonance; RER, respiratory exchange ratio; SDS-PAGE, sodium dodecyl sulfate-polyacrylamide gel electrophoresis; TLC, thin-layer chromatography; VO_2, oxygen consumption; VCO_2, carbon dioxide production. Ganglioside nomenclature is that of Svennerholm (1994).

References

Aerts JM, Ottenhoff R, Powlson AS, Grefhorst A, van Eijk M, Dubbelhuis PF, Aten J, Kuipers F, Serlie MJ, Wennekes T, et al. 2007. Pharmacological inhibition of glucosylceramide synthase enhances insulin sensitivity. *Diabetes*. 56:1341–1349.

Allende ML, Proia RL. 2014. Simplifying complexity: genetically resculpting glycosphingolipid synthesis pathways in mice to reveal function. *Glycoconj J*. 31:613–622.

Anumula KR, Taylor PB. 1992. A comprehensive procedure for preparation of partially methylated alditol acetates from glycoprotein carbohydrates. *Anal Biochem*. 203:101–108.

Aoki K, Perlman M, Lim JM, Cantu R, Wells L, Tiemeyer M. 2007. Dynamic developmental elaboration of N-linked glycan complexity in the Drosophila melanogaster embryo. *J Biol Chem*. 282:9127–9142.

Audry M, Jeanneau C, Imberty A, Harduin-Lepers A, Delannoy P, Breton C. 2011. Current trends in the structure-activity relationships of sialyltransferases. *Glycobiology*. 21:716–726.

Bauer J, Osborn HM. 2015. Sialic acids in biological and therapeutic processes: opportunities and challenges. *Future Med Chem*. 7:2285–2299.

Cohen M, Varki A. 2010. The sialome—far more than the sum of its parts. *OMICS*. 14:455–464.

Ellies LG, Sperandio M, Underhill GH, Yousif J, Smith M, Priatel JJ, Kansas GS, Ley K, Marth JD. 2002. Sialyltransferase specificity in selectin ligand formation. *Blood*. 100:3618–3625.

Guo S. 2014. Insulin signaling, resistance, and the metabolic syndrome: insights from mouse models into disease mechanisms. *J Endocrinol*. 220: T1–T23.

Holland WL, Knotts TA, Chavez JA, Wang LP, Hoehn KL, Summers SA. 2007. Lipid mediators of insulin resistance. *Nutr Rev*. 65:S39–S46.

Inokuchi J. 2014. GM3 and diabetes. *Glycoconj J*. 31:193–197.

Iwamori M, Shimomura J, Tsuyuhara S, Nagai Y. 1984. Gangliosides of various rat tissues: distribution of ganglio-N- tetraose-containing gangliosides and tissue-characteristic composition of gangliosides. *J Biochem (Tokyo)*. 95:761–770.

Kabayama K, Sato T, Saito K, Loberto N, Prinetti A, Sonnino S, Kinjo M, Igarashi Y, Inokuchi J. 2007. Dissociation of the insulin receptor and caveolin-1 complex by ganglioside GM3 in the state of insulin resistance. *Proc Natl Acad Sci. U S A*. 104:13678–13683.

Kaucic K, Liu Y, Ladisch S. 2006. Modulation of growth factor signaling by gangliosides: positive or negative? *Methods Enzymol*. 417:168–185.

Keranen A. 1976. Fatty acids and long-chain bases of gangliosides of human gastrointestinal mucosa. *Chem Phys Lipids*. 17:14–21.

Lipina C, Hundal HS. 2015. Ganglioside GM3 as a gatekeeper of obesity-associated insulin resistance: Evidence and mechanisms. *FEBS Lett*. 589: 3221–3227.

Lipina C, Nardi F, Grace H, Hundal HS. 2015. NEU3 sialidase as a marker of insulin sensitivity: Regulation by fatty acids. *Cell Signal*. 27:1742–1750.

Liu Y, Su Y, Wiznitzer M, Epifano O, Ladisch S. 2008. Ganglioside depletion and EGF responses of human GM3 synthase-deficient fibroblasts. *Glycobiology*. 18:593–601.

Lopez PH, Schnaar RL. 2006. Determination of glycolipid-protein interaction specificity. *Methods Enzymol*. 417:205–220.

Lusk G. 1928. *Elements of the Science of Nutrition*, 4th ed. Philadelphia and London, W.B. Saunders Co. p. 844.

Mitsuda T, Furukawa K, Fukumoto S, Miyazaki H, Urano T, Furukawa K. 2002. Overexpression of ganglioside GM1 results in the dispersion of platelet-derived growth factor receptor from glycolipid-enriched microdomains and in the suppression of cell growth signals. *J Biol Chem*. 277: 11239–11246.

Nagafuku M, Sato T, Sato S, Shimizu K, Taira T, Inokuchi J. 2015. Control of homeostatic and pathogenic balance in adipose tissue by ganglioside GM3. *Glycobiology*. 25:303–318.

Nimrichter L, Burdick MM, Aoki K, Laroy W, Fierro MA, Hudson SA, Von Seggern CE, Cotter RJ, Bochner BS, Tiemeyer M, et al. 2008. E-selectin receptors on human leukocytes. *Blood*. 112:3744–3752.

Nojiri H, Stroud M, Hakomori S. 1991. A specific type of ganglioside as a modulator of insulin- dependent cell growth and insulin receptor tyrosine kinase activity. Possible association of ganglioside-induced inhibition of insulin receptor function and monocytic differentiation induction in HL-60 cells. *J Biol Chem*. 266:4531–4537.

Ohashi M. 1979. A comparison of the ganglioside distributions of fat tissues in various animals by two-dimensional thin layer chromatography. *Lipids*. 14:52–57.

Pan B, Fromholt SE, Hess EJ, Crawford TO, Griffin JW, Sheikh KA, Schnaar RL. 2005. Myelin-associated glycoprotein and complementary axonal ligands, gangliosides, mediate axon stability in the CNS and PNS: neuropathology and behavioral deficits in single- and double-null mice. *Exp Neurol*. 195:208–217.

Park JW, Park WJ, Kuperman Y, Boura-Halfon S, Pewzner-Jung Y, Futerman AH. 2013. Ablation of very long acyl chain sphingolipids causes hepatic insulin resistance in mice due to altered detergent-resistant membranes. *Hepatology*. 57:525–532.

Rohrer JS. 2000. Analyzing sialic acids using high-performance anion-exchange chromatography with pulsed amperometric detection. *Anal Biochem*. 283:3–9.

Saltiel AR. 2016. Insulin signaling in the control of glucose and lipid homeostasis. *Handb Exp Pharmacol*. 233:51–71.

Sasaki A, Hata K, Suzuki S, Sawada M, Wada T, Yamaguchi K, Obinata M, Tateno H, Suzuki H, Miyagi T. 2003. Overexpression of plasma membrane-associated sialidase attenuates insulin signaling in transgenic mice. *J Biol Chem*. 278:27896–27902.

Sasaki N, Itakura Y, Toyoda M. 2015. Ganglioside GM1 contributes to the state of insulin resistance in senescent human arterial endothelial cells. *J Biol Chem*. 290:25475–25486.

Schauer R. 2009. Sialic acids as regulators of molecular and cellular interactions. *Curr Opin Struct Biol*. 19:507–514.

Schnaar RL. 1994. Isolation of glycosphingolipids. *Methods Enzymol*. 230: 348–370.

Schnaar RL. 2016. Gangliosides of the vertebrate nervous system. *J Mol Biol*. 427:3325–3336.

Schnaar RL, Gerardy-Schahn R, Hildebrandt H. 2014. Sialic acids in the brain: gangliosides and polysialic acid in nervous system development, stability, disease and regeneration. *Physiol Rev*. 94:461–518.

Schnaar RL, Needham LK. 1994. Thin-layer chromatography of glycosphingolipids. *Methods Enzymol*. 230:371–389.

Sonnino S, Prinetti A. 2010. Gangliosides as regulators of cell membrane organization and functions. *Adv Exp Med Biol*. 688:165–184.

Sturgill ER, Aoki K, Lopez PH, Colacurcio D, Vajn K, Lorenzini I, Majic S, Yang WH, Heffer M, Tiemeyer M, et al. 2012. Biosynthesis of the major brain gangliosides GD1a and GT1b. *Glycobiology*. 22: 1289–1301.

Svennerholm L. 1994. Designation and schematic structure of gangliosides and allied glycosphingolipids. *Prog Brain Res*. 101:xi–xiv.

Tagami S, Inokuchi JJ, Kabayama K, Yoshimura H, Kitamura F, Uemura S, Ogawa C, Ishii A, Saito M, Ohtsuka Y, et al. 2002. Ganglioside GM3 participates in the pathological conditions of insulin resistance. *J Biol Chem*. 277:3085–3092.

Tanabe A, Matsuda M, Fukuhara A, Miyata Y, Komuro R, Shimomura I, Tojo H. 2009. Obesity causes a shift in metabolic flow of gangliosides in adipose tissues. *Biochem Biophys Res Commun*. 379:547–552.

Taniguchi N, Honke K, Fukuda M, Narimatsu H, Yamaguchi Y, Angata T. 2014. *Handbook of Glycosyltransferases and Related Genes*, 2nd ed. Tokyo, Springer. p. 1707.

Todeschini AR, Hakomori SI. 2008. Functional role of glycosphingolipids and gangliosides in control of cell adhesion, motility, and growth, through glycosynaptic microdomains. *Biochim Biophys Acta*. 1780: 421–433.

Tsuji S, Takashima S. 2014. ST3 beta-galactoside alpha-2,3-sialyltransferase 2 (ST3GAL2). In: Taniguchi N, Honke K, Fukuda M, Narimatsu H, Yamaguchi Y, Angata T editors. *Handbook of Glycosyltransferases and Related Genes*, 2nd ed. Tokyo, Springer. p. 645–656.

van Eijk M, Aten J, Bijl N, Ottenhoff R, van Roomen CP, Dubbelhuis PF, Seeman I, Ghauharali-van der Vlught Karen, Overkleeft HS, Arbeeny C, et al. 2009. Reducing glycosphingolipid content in adipose tissue of obese mice restores insulin sensitivity, adipogenesis and reduces inflammation. *PLoS ONE*. 4:e4723.

Varki A, Cummings RD, Aebi M, Packer NH, Seeberger PH, Esko JD, Stanley P, Hart G, Darvill A, Kinoshita T, et al. 2015. Symbol nomenclature for graphical representations of glycans. *Glycobiology*. 25: 1323–1324.

Veillon L, Go S, Matsuyama W, Suzuki A, Nagasaki M, Yatomi Y, Inokuchi J. 2015. Identification of ganglioside GM3 molecular species in human serum associated with risk factors of metabolic syndrome. *PLoS ONE*. 10:e0129645.

Vukelic Z, Zamfir AD, Bindila L, Froesch M, Peter-Katalinic J, Usuki S, Yu RK. 2005. Screening and sequencing of complex sialylated and sulfated glycosphingolipid mixtures by negative ion electrospray Fourier transform ion cyclotron resonance mass spectrometry. *J Am Soc Mass Spectrom*. 16: 571–580.

Yamashita T, Hashiramoto A, Haluzik M, Mizukami H, Beck S, Norton A, Kono M, Tsuji S, Daniotti JL, Werth N, et al. 2003. Enhanced insulin sensitivity in mice lacking ganglioside GM3. *Proc Natl Acad Sci. U S A*. 100:3445–3449.

Yew NS, Zhao H, Hong EG, Wu IH, Przybylska M, Siegel C, Shayman JA, Arbeeny CM, Kim JK, Jiang C, et al. 2010. Increased hepatic insulin action in diet-induced obese mice following inhibition of glucosylceramide synthase. *PLoS ONE*. 5:e11239.

Yoo SW, Motari MG, Susuki K, Prendergast J, Mountney A, Hurtado A, Schnaar RL. 2015. Sialylation regulates brain structure and function. *FASEB J*. 29:3040–3053.

Zakharova IO, Sokolova TV, Vlasova YA, Furaev VV, Rychkova MP, Avrova NF. 2014. GM1 ganglioside activates ERK1/2 and Akt downstream of Trk tyrosine kinase and protects PC12 cells against hydrogen peroxide toxicity. *Neurochem Res*. 39:2262–2275.

Zhao H, Przybylska M, Wu IH, Zhang J, Siegel C, Komarnitsky S, Yew NS, Cheng SH. 2007. Inhibiting glycosphingolipid synthesis improves glycemic control and insulin sensitivity in animal models of type 2 diabetes. *Diabetes*. 56:1210–1218.